1428 *Inorg. Chem.* **2010**, *49*, 1428–1432
DOI: 10.1021/ic9015417

Inorganic Chemistry
Article

Stabilization of Long-Lived Metastable State in Long Alkylated Spin-Crossover Cobalt(II) Compound

Shinya Hayami,*,† Daisuke Urakami,‡ Yoshihiro Kojima,‡ Hokuto Yoshizaki,‡ Yuuki Yamamoto,† Kazuya Kato,† Akira Fuyuhiro,§ Satoshi Kawata,∥ and Katsuya Inoue‡

†*Department of Chemistry, Graduate School of Science and Technology, Kumamoto University, 2-39-1 Kurokami, Kumamoto, 860-8555 Japan,* ‡*Department of Chemistry, Graduate School of Science, Hiroshima University, 1-3-1 Kagamiyama, Higashi-hiroshima, 739-8526 Japan,* §*Department of Chemistry, Graduate School of Science, Osaka University, Toyonaka, Osaka, 560-0043 Japan, and* ∥*Department of Chemistry, Faculty of Science, Fukuoka University, 8-19-1 Nakamura, Jonan-ku, Fukuoka, 814-0180 Japan*

Received August 3, 2009

The A mixed crystal compound $[Co_{0.8}Fe_{0.2}(C16\text{-terpy})_2](BF_4)_2$ (**2**) (C16-terpy is 4′-hexadecyloxy-2,2′:6′,2″-terpyridine) with long alkyl chains was prepared by mixing $[Co(C16\text{-terpy})_2](BF_4)_2$ (**1**), which exhibits unique magnetic behavior, and the diamagnetic iron(II) compound $[Fe(C16\text{-terpy})_2](BF_4)_2$ (**3**). The long-lived metastable state in the frozen-in effect was observed for the first time in the spin-crossover cobalt(II) compound **2**. Furthermore, relaxation from metastable to stable states was very slow because of a large structural transition resulting from the long alkyl chains.

Introduction

Flexible and soft molecules are the focus of materials research for functional device construction for polymers, films, gels, and liquid crystals.[1−4] Soft materials are very interesting for both their application as functional materials and their phase transitions. Construction of metal complexes with long alkyl chains allows investigation of their flexible spaces and central metal complexes. Synchronicity may be observed between the central metal complexes and the long alkyl chains that surround them. Gaspar et al. investigated the synchronicity of transition, spin transition, and solid−liquid crystal transition in iron(II) complexes.[5] Chang et al. reported a synchronic bistability of valence tautomerism and crystal-melt phase transition.[6] We have previously investigated the possibility of synchronization between the motion of long alkyl chains and spin states.[7−11] Placing a metal complex with spin-crossover (SCO) in the flexible and soft space formed by long alkyl chains is expected to produce novel physical properties due to synergy between SCO and the response of the flexible field toward external stimuli.

The SCO cobalt(II) compounds exhibit a $1/2 \leftrightarrow 3/2$ spin change. It has been known that the cobalt(II) compounds $[Co(terpy)_2]X_2 \cdot nH_2O$ (terpy = 2,2′:6′,2″-terpyridine, X = halide, pseudohalide, NO_3^-, ClO_4^-, and $n = 0-5$) exhibit incomplete and gradual SCO behavior.[12,13] Recently, we suggested that cooperativity in soft materials produces novel switching functions and reported that the long alkylated cobalt(II) compound $[Co(C16\text{-terpy})_2](BF_4)_2$ (**1**) (C16-terpy is 4′-hexadecyloxy-2,2′:6′,2″-terpyridine) exhibits a "reverse spin transition" between high-spin (HS) and low-spin (LS) with a thermal hysteresis loop triggered by a structural phase transition.[8] To establish cooperativity in the SCO cobalt(II) compound **1**, we recently investigated the percolation of intermolecular interactions when mixing diamagnetic molecules with **1**. Generally, the percolation effect in mixed-crystal systems decreased the domain size and weakened cooperativity. However, some unique behaviors have also been

*To whom correspondence should be addressed. E-mail: hayami@sci.kumamoto-u.ac.jp.

(1) Cobo, S.; Molnár, G.; Real, J. A.; Bousseksou, A. *Angew. Chem., Int. Ed.* **2006**, *45*, 5786.
(2) Létard, J. F.; Nbuyen, O.; Soyer, H.; Mingotaud, C.; Delhaès, P.; Kahn, O. *Inorg. Chem.* **1999**, *38*, 3020.
(3) Kuroiwa, K.; Shibata, T.; Takada, A.; Nemoto, N.; Kimizuka, N. *J. Am. Chem. Soc.* **2004**, *126*, 2016.
(4) Ha, N. Y.; Ohtsuka, Y.; Jeong, S. M.; Nishimura, S.; Suzaki, G.; Takanishi, Y.; Ishikawa, K.; Takezoe, H. *Nat. Mater.* **2008**, *7*, 43.
(5) Seredyuk, M.; Gaspar, A. B.; Ksenofontov, V.; Galyametdinov, Y.; Kusz, J.; Gütlich, P. *J. Am. Chem. Soc.* **2008**, *130*, 1431.
(6) Kiriya, D.; Chang, H. C.; Kitagawa, S. *J. Am. Chem. Soc.* **2008**, *130*, 5515.
(7) Hayami, S.; Danjobara, K.; Inoue, K.; Ogawa, Y.; Matsumoto, N.; Maeda, Y. *Adv. Mater.* **2004**, *16*, 869.
(8) Hayami, S.; Shigeyoshi, Y.; Akita, M.; Inoue, K.; Kato, K.; Osaka, K.; Takata, M.; Kawajiri, R.; Mitani, T.; Maeda, Y. *Angew. Chem., Int. Ed.* **2005**, *44*, 4899.
(9) Hayami, S.; Moriyama, R.; Shigeyoshi, Y.; Kawajiri, R.; Mitani, T.; Akita, M.; Inoue, K.; Maeda, Y. *Inorg. Chem.* **2005**, *44*, 7295.
(10) Hayami, S.; Motokawa, N.; Shuto, A.; Someya, T.; Ogawa, Y.; Inoue, K.; Maeda, Y. *Inorg. Chem.* **2007**, *46*, 1789.
(11) Hayami, S.; Moriyama, R.; Shuto, A.; Maeda, Y.; Ohta, K.; Inoue, K. *Inorg. Chem.* **2007**, *46*, 7692.
(12) Judge, J. S.; Baker, W. A., Jr. *Inorg. Chim. Acta* **1967**, *1*, 68.
(13) Kremer, S.; Henke, W.; Reinen, D. *Inorg. Chem.* **1982**, *21*, 3013.

 Published on Web 01/12/2010

reported, such as an increased hysteresis loop and observation of a photoinduced spin transition in the LS compound.[14,15] For this purpose, we have focused on the mixed-crystal compound $[Co_{0.8}Fe_{0.2}(C16\text{-terpy})_2](BF_4)_2$ (**2**) obtained by mixing the spin transition cobalt(II) compound $[Co(C16\text{-terpy})_2](BF_4)_2$ (**1**) and the diamagnetic iron(II) compound $[Fe(C16\text{-terpy})_2](BF_4)_2$ (**3**).[16] In this paper, we report on the appearance of a metastable phase in **2**. This is the first reported observation of a "frozen-in" effect caused by rapid cooling for the SCO cobalt(II) compounds. Inordinately slow relaxation from the metastable LS to original HS states was also observed due to large structural change resulting from the long alkyl chains.

Experimental Section

Synthesis. All reagents were commercially available and used without further purification. The complexes $[Co(C16\text{-terpy})_2](BF_4)_2$ (**1**) and $[Fe(C16\text{-terpy})_2](BF_4)_2$ (**3**) were prepared according to the methods described previously.[8,16] Mixed-crystal powder samples $[Co_{0.8}Fe_{0.2}(C16\text{-terpy})_2](BF_4)_2$ (**2**) were obtained by mixing theoretical amounts of **1** and **3** in ethanol (EtOH). Single crystals of **2**·EtOH, suitable for X-ray diffraction (XRD) analysis, were isolated as EtOH adducts by slow recrystallization from EtOH. Elem anal. for **2**·EtOH calcd for $C_{64}H_{92}O_3N_6B_2F_8Fe_{0.2}Co_{0.8}$: C, 62.73; H, 7.57; N, 6.86. Found: C, 62.92; H, 7.55; N, 7.01. Compound **2** was obtained by annealing **2**·EtOH at 400 K. Anal. calcd for $C_{62}H_{86}O_2N_6B_2F_8Co_{0.8}Fe_{0.2}$ (**2**): C, 63.14; H, 7.35; N, 7.13. Found: C, 62.93; H, 7.57; N, 7.24. Other mixed-crystal samples, $[Co_{0.9}Fe_{0.1}(C16\text{-terpy})_2](BF_4)_2$, $[Co_{0.7}Fe_{0.3}(C16\text{-terpy})_2](BF_4)_2$, and $[Co_{0.6}Fe_{0.4}(C16\text{-terpy})_2](BF_4)_2$, were obtained by mixing theoretical amounts of **1** and **3** in ethanol (EtOH). The elemental analyses for $[Co_{0.9}Fe_{0.1}(C16\text{-terpy})_2](BF_4)_2$ are as follows. Anal. calcd for $C_{62}H_{86}O_2N_6B_2F_8Co_{0.9}Fe_{0.1}$: C, 63.19; H, 7.35; N, 7.12. Found: C, 62.99; H, 7.55; N, 7.21. The elemental analyses for $[Co_{0.7}Fe_{0.3}(C16\text{-terpy})_2](BF_4)_2$ are as follows. Anal. calcd for $C_{62}H_{86}O_2N_6B_2F_8Co_{0.7}Fe_{0.3}$: C, 63.16; H, 7.35; N, 7.13. Found: C, 62.89; H, 7.48; N, 7.19. The elemental analyses for $[Co_{0.6}Fe_{0.4}(C16\text{-terpy})_2](BF_4)_2$ are as follows. Anal. calcd for $C_{62}H_{86}O_2N_6B_2F_8Co_{0.6}Fe_{0.4}$: C, 63.18; H, 7.35; N, 7.13. Found: C, 63.01; H, 7.41; N, 7.09.

Susceptibility Measurements. The magnetic susceptibilities $\chi(T)$ for **2** between 5 and 400 K were measured with a superconducting quantum interference device magnetometer (Quantum Design MPMS-5S) in an external field of 1.0 T.

Mössbauer Spectroscopy. The Mössbauer spectra (isomer shift versus metallic iron at room temperature) were measured with a Wissel MVT-1000 Mössbauer spectrometer with a ^{57}Co/Rh source in the transmission mode. All isomer shifts are given relative to α-Fe at room temperature. Measurements at low temperatures were performed with a closed-cycle helium refrigerator cryostat (Iwatani Co., Ltd.). In order to enhance the Mössbauer spectra, the sample was enriched with ^{57}Fe.

Crystallographic Data Collection and Structure Determination. A single crystal of **2**·EtOH was mounted on a glass fiber. The temperature of the crystals was slowly decreased from room temperature down to 100 K. Then, X-ray structural analysis was carried out. The measurement was performed on a Bruker SMART-APEX diffractometer equipped with a CCD area detector and graphite-monochromated Mo K_α radiation, λ = 0.71073A°, ω-scan mode (0.3° steps). Semiempirical absorption corrections on Laue equivalents were applied. The structure was solved by direct methods and refined by full-matrix least squares against F^2 of all data using SHELX-97. Non-hydrogen atoms were refined anisotropically. Hydrogen atoms were included but not refined.

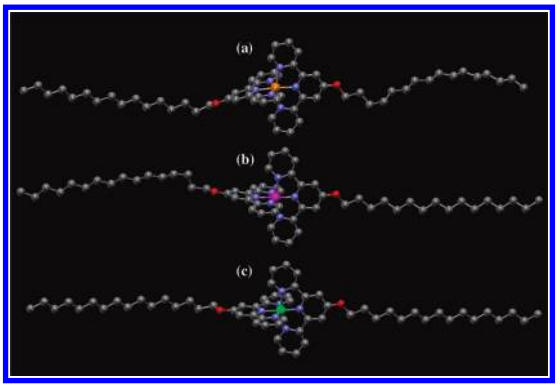

Figure 1. Single crystal structures for (a) **1**·MeOH, (b) **2**·EtOH, and (c) **3**·acetone at 100 K. Counter anions, solvent molecules, and hydrogen atoms are omitted for clarity.

Powder X-Ray Diffraction Measurement. Powder X-ray diffraction (XRD) patterns were obtained on a Rigaku 2100 diffractometer at room temperature with Cu Kα radiation in a flat-plate geometry. Further, to obtain X-ray powder data of good statistics with high angular resolution, XRD measurements were carried out at the Spring-8, BL02B2 beamline (temperature dependence and illumination effect) at 150 to 300 K. The as-grown sample powders were fine enough and gave a homogeneous intensity distribution in the Debye−Scherrer powder ring. At the BL02B2 beamline, the sample powders were sealed in a glass capillary. The reflections were collected on an imaging plate installed on a large Debye−Scherrer camera (r = 286.5 nm). The wavelength of the incident X-ray was about 1.0 Å (near below the K edge of Rb), and typical exposure time was 15 min. Actual wavelength was calibrated with the use of a standard CeO_2 powder obtained from NIST.

Results and Discussion

The structures of **1**·MeOH and **3**·acetone were determined previously (Figures 1 (a) and (c)).[8,16] The single crystal structure for **2**·EtOH was also determined at 100 K. **2·EtOH** had a similar structure to **1**·MeOH and **3**·acetone, and also crystallized in the triclinic *P-1* space group (Figure 1 (b)). The single-crystal X-ray analysis for **2**·EtOH revealed that each of the cobalt(II) atoms are octahedrally coordinated by six nitrogen atoms in two C16-terpy ligands, that is, an N_6 donor set. The Co−N distances of the central pyridine in the terpyridine unit are Co−N(2) = 1.944(5) Å and Co−N(5) = 1.901(5) Å. On the other hand, for the Co−N distances of the side pyridines in the terpyridine unit, remarkable differences are noted between the N(1)∩N(3) side and the N(4)∩N(6) side. The average Co−N distance of Co−N(1) and Co−N(3) is 2.13 Å, and that of Co−N(4) and Co−N(6) is 2.03 Å. The distance in the N(1)∩N(3) side is longer than that in the N(4)∩N(6) side. The values of the bond lengths are intermediate between those for typical LS and HS cobalt(II) compounds.[17−20] The Co−N distances of the central pyridine in

(14) Létard, J. F.; Capes, L.; Chastanet, G.; Molinar, N.; Létard, S.; Real, J. A.; Kahn, O. *Chem. Phys. Lett.* **1999**, *313*, 115.
(15) Renz, F.; Oshio, H.; Ksenofontov, V.; Waldeck, M.; Spiering, H.; Gütlich, P. *Angew. Chem., Int. Ed. Engl.* **2000**, *39*, 3699.
(16) Hayami, S.; Danjobara, K.; Shigeyoshi, Y.; Inoue, K.; Ogawa, Y.; Maeda, Y. *Inorg. Chem. Commun.* **2005**, *8*, 506.
(17) Gaspar, A. B.; Munoz, M. C.; Niel, V.; Real, J. A. *Inorg. Chem.* **2001**, *40*, 9.
(18) Zarembowitch, J.; Claude, R.; Kahn, O. *Inorg. Chem.* **1985**, *24*, 1576.
(19) Goodwin, H. A. *Top. Curr. Chem.*; Gütlich, P., Goodwin, H. A., Eds.; Springer-Verlag: Berlin, 2004; Vol. *234*, p 23.
(20) Hayami, S.; Murata, K.; Urakami, D.; Kojima, Y.; Akita, M.; Inoue, K. *Chem. Commun.* **2008**, 6510.

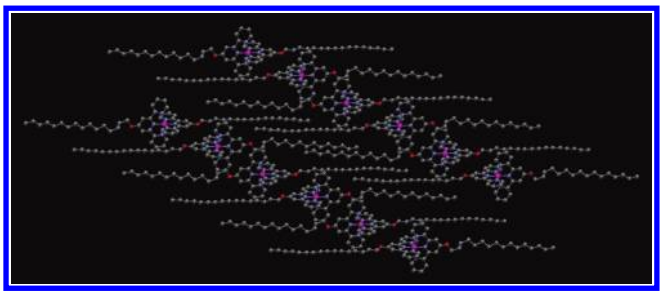

Figure 2. Projection of the crystal structure of **2**·EtOH along the *a* axis. Hydrogen atoms, counteranions, and solvent molecules are omitted for clarity.

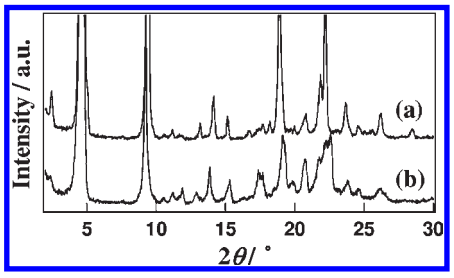

Figure 3. Powder XRD patterns (a) for **2** and (b) for **2**·EtOH at room temperature.

the terpyridine unit are shorter than that of the side pyridine in terpyridine unit, which induce a pronounced distortion of the CoN_6 octahedron. Three pyridine rings in the C16-terpy ligand are in the coplane, and the two tridentate C16-terpy ligands in the compound are found to be nearly perpendicular to one another. The long alkyl chains, $C_{16}H_{33}O$, are stuck out of 4′ position in the terpyridine moiety. Comparing **1**·MeOH, **2**·EtOH, and **3**·acetone allowed us to study the structure of the dication unit. The long alkyl chains ($C_{16}H_{33}O$) formed rod-like structures and protruded from the 4′ position of the terpyridine moiety for all compounds. For **2**·EtOH, one long alkyl chain was curved a small amount compared to that in **1**·MeOH. For **3**·acetone, the two long alkyl chains were straight in the rod-like formation. In this case, the two tridentate ligands were perpendicular to one another.

The two counteranions BF_4^- and one EtOH molecule are located in the intermolecular space, and there are short contacts between $[Co(C16\text{-terpy})_2]^{2+}$ cations, the BF_4^- anions, and EtOH molecules. $[Co_{0.8}Fe_{0.2}(C16\text{-terpy})_2]^{2+}$ cations formed $\pi-\pi$ interactions (3.40 Å) through the side pyridine and nearest neighbor pyridine rings (Figure 2). Further, there is fastener effect between the chains which faced each other in the complexes. The molecular packing of **2**·EtOH was very tight. This suggests that there are strong intermolecular interactions in the molecular assembly. The crystal structure of the nonsolvated compound **2** could not be determined because removal of EtOH molecules induced cracks in the crystal, making an X-ray single-crystal study impossible. However, powder XRD measurement suggested that the structure of nonsolvated **2** was similar to that of solvated **2**·EtOH (Figure 3). The phase purity for **2** was examined by comparing the powder XRD patterns for **1** and **3** (Figure S1, Supporting Information). The pattern for **2** ($Co_{0.8}Fe_{0.2}$) is rather close to that for **3** (pure Fe) but not that for **1** (pure Co), though the iron fraction is only 0.2.

The temperature dependences of the magnetic susceptibility for the solvated compound **2**·EtOH and nonsolvated

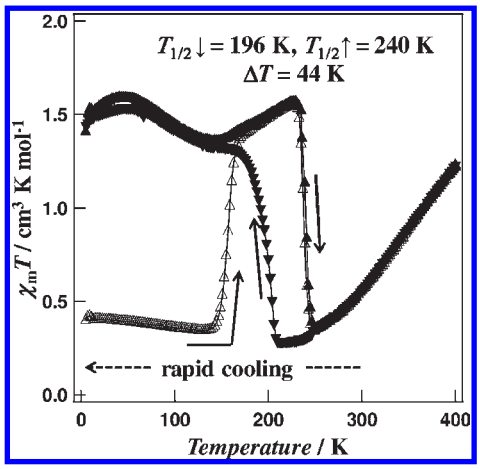

Figure 4. The observed $\chi_m T$ versus T plot of **2**, where the black triangles (▲ and ▼) show heating and cooling at 0.5 K min^{-1} and the red triangles (△) show heating at 0.5 K min^{-1} after the sample was rapidly cooled.

compound **2** were measured in the form of the $\chi_m T$ versus T curve, where χ_m is the molar magnetic susceptibility and T is the temperature. The solvated compound **2**·EtOH exhibited gradual SCO behavior in the temperature range of 5−360 K (Figure S2, Supporting Information). The $\chi_m T$ value for **2**·EtOH gradually increases from 0.54 cm^3 K mol^{-1} to 1.83 cm^3 K mol^{-1} at 360 K, and then the $\chi_m T$ value decreases to 1.58 cm^3 K mol^{-1} at 400 K because of removal of the EtOH molecules. Magnetic behaviors for **1** and **3** were reported previously.[8,16] Compound **1** exhibited unique magnetic behavior with a reverse spin transition ($T_{1/2}\downarrow$ = 217 K and $T_{1/2}\uparrow$ = 260 K) and thermal hysteresis loop (ΔT = 43 K). Compound **3** was in the LS state from 5 to 400 K. Figure 4 shows the product of the molar magnetic susceptibility (χ_m) and temperature (T) plotted against T. The $\chi_m T$ value for **2** gradually decreased from 1.22 cm^3 K mol^{-1} at 400 K to 0.28 cm^3 K mol^{-1} at 212 K. Powder XRD patterns for **2** were measured at 300, 350, and 400 K (Figure S3, Supporting Information). The peaks of the patterns move to the low-angle side as the temperature rises, and it is suggested that the molecules expand. The cobalt(II) compounds $[Co(terpy)_2]X_2 \cdot nH_2O$ show gradual SCO behavior between 0.44 and 0.54 cm^3 K mol^{-1} at low temperatures and 2.00 and 2.80 cm^{3}Kmol^{-1} at high temperatures for the $\chi_m T$ value, and this gradual decrease in $\chi_m T$ may indicate thermal SCO behavior.[12,13] On further cooling, $\chi_m T$ increased abruptly at around $T_{1/2}\downarrow$ = 196 K to 1.33 cm^3 K mol^{-1} at 156 K, showing the transition from LS to HS states. On heating, $\chi_m T$ abruptly dropped at around $T_{1/2}\uparrow$ = 240 K, showing the transition from HS to LS states. This magnetic behavior shows that compound **2** also exhibits a reverse spin transition at $T_{1/2}\downarrow$ = 196 K and $T_{1/2}\uparrow$ = 240 K with wide thermal hysteresis (ΔT = 44 K).

Mössbauer spectra for **2** were measured at various temperatures (Figure 5). The spectra gave the parameters $Q.S.$ = 1.18 mm s^{-1} and $I.S.$ = 0.282 mm s^{-1} at 80 K and $Q.S.$ = 1.18 mm s^{-1} and $I.S.$ = 0.263 mm s^{-1} at 200 K and showed the LS state for the iron(II) ions in **2**. Therefore, it is suggested that the magnetic behavior of **2** results from cobalt(II) ions. Powder XRD measurements suggested that the HS structure at 150 K was very different from the LS structure at 300 K. It is thought that a large structure phase transition occurred from 150 to 300 K (Figure S4, Supporting Information).

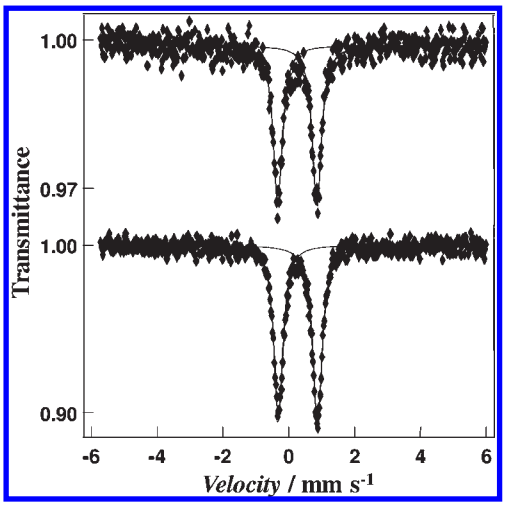

Figure 5. Mössbauer spectra for **2** at (a) 200 and (b) 80 K.

Thermogravimetric data for **2** were collected on a SII DSC 6100 instrument over the 150−300 K temperature range at a rate of 5 K min^{-1} because the the differential scanning calorimetry (DSC) peaks from measurement at a slow scan rate were difficult to observe. On warming, three endothermic peaks were observed at 217, 239, and 251 K in DSC. The peak at 239 K corresponded to the spin transition temperature ($T_{1/2}\uparrow$ = 240 K; Figure S5, Supporting Information). On cooling, two peaks were observed at 199 and 249 K, and the 199 K peak corresponded to the spin transition temperature ($T_{1/2}\downarrow$ = 196 K). It is thought that other peaks may be assigned to some kind of structural phase transitions accompanied by moving of the long alkyl chains.

The sample was rapidly quenched in the liquid-helium-temperature cavity of the SQUID equipment, and this cooled the sample within a few seconds. After quenching, $\chi_m T$ was 0.40 cm^3 K mol^{-1}, showing that the LS state was frozen-in.[21−24] A slight relaxation to the HS state was not observed even after days. The sample was then slowly warmed up and the metastable frozen-in LS state relaxed back to the original HS state at T_{relax} = 157 K. This was observed when the cooperativity was large, and therefore the relaxation rate from metastable to stable states was quite slow.[25] The bistable states, metastable LS and HS, existed below 140 K. The cobalt(II) compound **1** does not exhibit the frozen-in effect, but the mixed-crystal compound **2** does because a new phase state appears due to dilution with the diamagnetic iron(II) compound **3**. Magnetic behaviors for compounds at other ratios, $[Co_xFe_{1-x}(C16\text{-terpy})_2](BF_4)_2$ (x = 0.9, 0.7, 0.6), were also measured (Figures S6−S8, Supporting Information). The compounds with x = 0.9 and 0.7 also showed the frozen-in effect, but the compound with x = 0.6 did not. The frozen-in effect can be explained as follows. The ionic size of a LS iron(II) ion (0.75 Å) is much smaller than that of a HS cobalt(II) ion (0.89 Å). The presence of a significant amount of LS iron(II) ions in the lattice introduces a negative chemical pressure in the system. This helps create a more compact metastable LS cobalt(II) phase, and the frozen-in effect works better with a higher ratio of iron, as in $Co_{0.8}Fe_{0.2}$ compared with $Co_{0.9}Fe_{0.1}$. Further increases in the LS iron(II) ion content lead to suppression of the reverse spin transition. The frozen-in effect then disappears due to suppression of the reverse spin transition. This is clearly seen when comparing samples $Co_{0.7}Fe_{0.3}$ and $Co_{0.6}Fe_{0.4}$. All of these observations can be explained by the negative chemical pressure introduced in the system when doped with a smaller cation like the LS iron(II) ion. With a high LS iron(II) ion content, the energy gained in the structural phase transition (reverse spin transition) cannot overcome the chemical pressure in the system, and the phenomenon is suppressed.

The LS → HS relaxation curves after the frozen-in effect for **2** are shown in the temperature range of 100−145 K, and the time dependence of the $\chi_m T$ values can be studied with the SQUID setup. Decay of the HS molar fraction (γ_{LS}) versus time at various temperatures for **2** is presented in (Figure S9, Supporting Information); γ_{LS} is deduced from the $\chi_m T$ value and normalized to unity at time 0. Analysis of these data indicates that the relaxation curves deviate from the single-exponential behavior shown in eq 1.

$$\gamma_{LS}(t) = \exp[-k_{LH}(T)t] \tag{1}$$

The time dependence of the LS molar fraction follows a sigmoidal-type behavior.[25−27] It is well established that the HS → LS relaxation for spin transition compounds in the solid state is strongly influenced by cooperative effects. Such curves can be interpreted as a self-acceleration of the LS → HS relaxation as γ_{LS} decreases. Each LS ion in a crystal acts as internal pressure (image pressure) and increases the relaxation rate. This internal pressure is caused by the large change in size of the SCO compound as it converts from the LS state into the HS state. The rate of disappearance of the LS fraction is given by eqs 2−4.

$$-\frac{d\gamma_{LS}}{dt} = k_{LH}(\gamma_{LS}, T)\gamma_{LS} \tag{2}$$

$$k_{LH}(\gamma_{LS}, T) = k_{LH}(T)\exp\left(-\frac{E_a^*}{k_B T}\gamma_{LS}\right) \tag{3}$$

$$k_{LH}(T) = k_{LH}^{\circ}\exp\left(-\frac{E_a}{k_B T}\right) \tag{4}$$

In eq 2, $k_{LH}(\gamma_{LS},T)$ is the rate constant for the LS → HS relaxation. This parameter is a function of γ_{LS} and T. E_a* stands for the additional activation energy due to cooperativity, and $k_{LH}(T)$ stands for the relaxation rate at T (eq 3). Finally, k_{LH}° is the preexponential factor, and E_a is the activation energy associated with the LS → HS relaxation (eq 4). The $k_{LH}(T)$ values at various temperatures in the range of 100−145 K were determined by using eqs 2−4. The parameters k_{LH}° and E_a are shown in Table 1, and Figure 6 presents the $\ln[k_{LH}(T)]$ versus $1/T$ plots for **2**. The $k_{LH}(T)$ is the rate constant for the metastable LS → HS relaxation.

(21) Buchen, Th.; Gütlich, P.; Goodwin, H. A. *Inorg. Chem.* **1994**, *33*, 4573.
(22) Hayami, S.; Maeda, Y. *Inorg. Chim. Acta* **1997**, *255*, 181.
(23) Nelson, S. M.; Mcllroy, P. D. A.; Stevenson, C. S.; König, E.; Ritter, G.; Waigel, J. *J. Chem. Soc., Dalton Trans.* **1986**, 991.
(24) Ritter, G.; König, E.; Irler, W.; Goodwin, H. A. *Inorg. Chem.* **1978**, *17*, 224.
(25) Hayami, S.; Hiki, K.; Kawahara, T.; Maeda, Y.; Urakami, D.; Inoue, K.; Ohama, M.; Kawata, S.; Sato, O. *Chem.—Eur. J.* **2009**, *15*, 3497.
(26) Hauser, A.; Adler, J.; Gütlich, P. *Chem. Phys. Lett.* **1988**, *152*, 468.
(27) Létard, J.-F. *J. Mater. Chem.* **2006**, *16*, 2550.

Table 1. Preexponential Factor k_{LH} and Activation Energy E_a

temperature	k_{LH}/s^{-1}	E_a/cm^{-1}
100 K	6.81×10^{-8}	317.08
110 K	4.43×10^{-7}	270.92
120 K	5.69×10^{-6}	150.69
125 K	9.95×10^{-6}	121.64
130 K	2.33×10^{-5}	64.24
135 K	4.58×10^{-5}	0.00
140 K	1.06×10^{-4}	0.00
145 K	3.54×10^{-4}	0.00

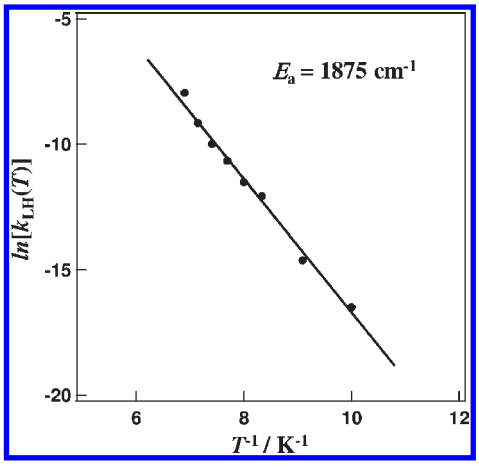

Figure 6. $\ln[k_{LH}(T)]$ versus T^{-1} curve. For $100 \leq T \leq 145$ K, a straight line is obtained with $E_a = 1875$ cm^{-1}.

Both thermally activated relaxation behavior at elevated temperatures and nearly temperature-independent relaxation behavior at low temperatures were observed. For $100 \leq T \leq 145$ K, the $\ln[k_{LH}(T)]$ versus $1/T$ plot is linear and can be satisfactorily fitted with an Arrhenius law with $E_a = 1875$ cm^{-1}. The value for **2** is unreasonably larger than the rate expected for the SCO compounds because it is accompanied by a large structural transition in the long alkyl chains. Therefore, relaxation back from the metastable state to the original state could be difficult, even below the comparatively high temperature of 100 K.

It is important to note that the frozen-in effect was previously believed to be impossible for SCO cobalt(II) compounds due to the small structural change associated with the spin transition.[28] The achievement of an anomalous long-lived metastable state is considered to be due to the presence of the strong intermolecular interactions between long alkyl chains.

Conclusions

In summary, we successfully observed the frozen-in effect in a SCO cobalt(II) compound for the first time. Furthermore, the addition of long alkyl chains to the SCO cobalt(II) compound prevented thermal relaxation from the metastable state and introduced strong cooperativity. We believe that our approach of introducing intermolecular interactions to trap the metastable state could be widely applied. Applications include the design of other metal compounds with the frozen-in effect and the design of a variety of switchable molecular compounds.

Acknowledgment. This work was supported by "Development of Molecular Devices in Ferroelectric Metallomesogens" in 2006 from New Energy and Industrial Technology Development Organization (NEDO) of Japan and Grant-in-Aids for Science Research (No. 20350028) from the Ministry of Education, Culture, Sports, Science and Technology of the Japanese Government.

Supporting Information Available: Crystallographic data (CIF) for **2**·EtOH and a PDF file containing further information about synthesis and Figures S1−S10. This material is available free of charge via the Internet at http://pubs.acs.org.

(28) Gütlich, P.; Hauser, A.; Spiering, H. *Angew. Chem., Int. Ed. Engl.* **1994**, *33*, 2024.